SUPPORTING INFORMATION

Free-solution Label-free Detection of α-crystallin Chaperone Interactions by Back-scattering Interferometry

Joey C. Latham[1⊥], Richard Stein[2], Darryl J. Bornhop[1] and Hassane S. Mchaourab[2*]*

[1] Department of Chemistry and The Vanderbilt Institute for Chemical Biology

Vanderbilt University

VU Station B 351822 Nashville, TN 37235-1822

darryl.bornhop@vanderbilt.edu, *fax* (615) 343-1234

[2] Department of Molecular Physiology and Biophysics

Vanderbilt University School of Medicine

2215 Garland Ave., 741 Light Hall, Nashville, TN 37232

hassane.mchaourab@Vanderbilt.Edu, *fax* (615) 343-1234

[⊥] Current address: Mass Spectrometry Research Center and Department of Biochemistry

Vanderbilt University School of Medicine

465 21st Avenue South, MRB III Suite 9160, Nashville, TN 37232-8575

* Corresponding authors

SUPPORTING INFORMATION

TABLE OF CONTENTS

Figure S1 Photolithographic Workflow.

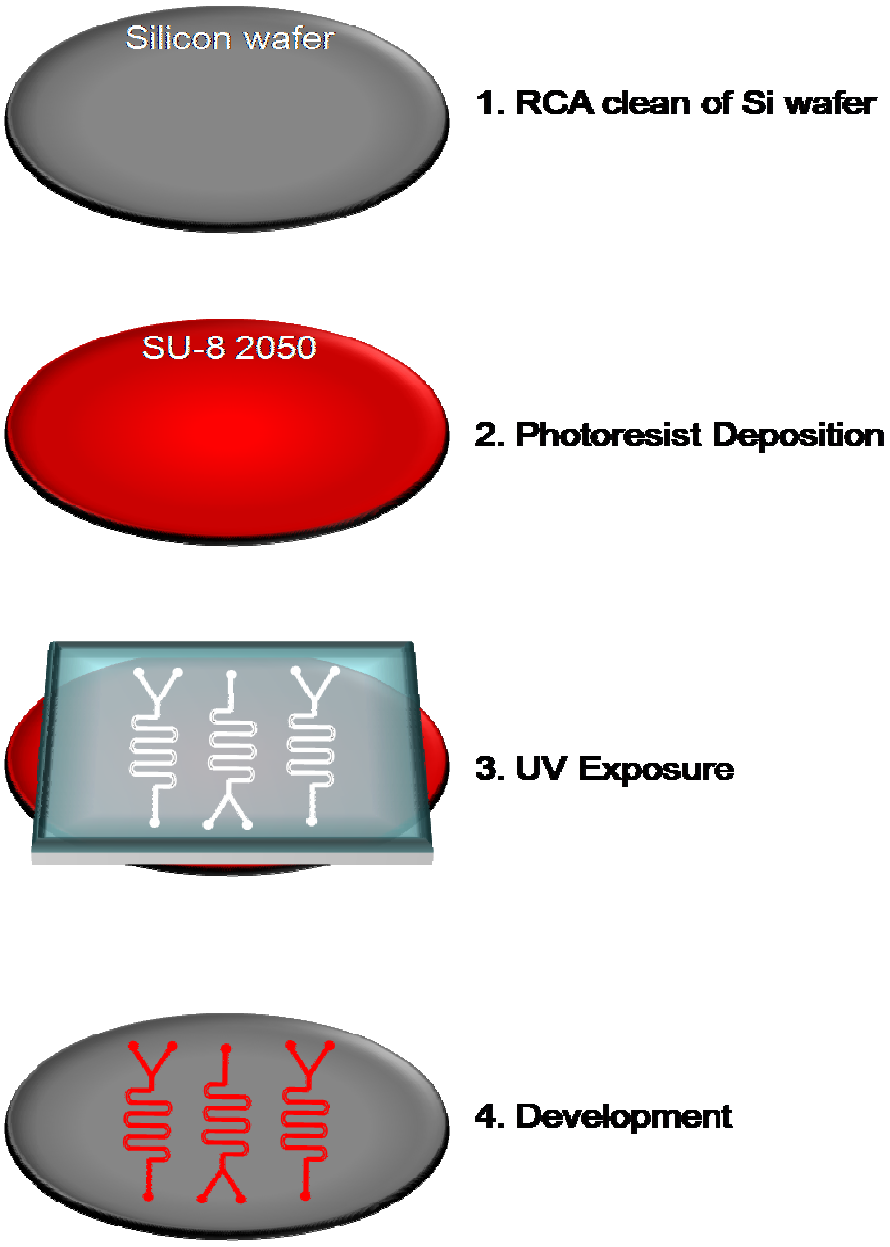

Figure S1 Photolithographic Workflow.

(1) Microchip fabrication began with the RCA cleaning of a 3″ silicon wafer. (2) The photoresist SU-8 2050 was then evenly deposited on the bare Si wafer using a Laurell spin-coater. (3) Following a short pre-bake, designed areas of photoresist were exposed to UV radiation through a soda lime/chrome mask. (4) After a short post-exposure bake, the silicon wafer was developed in an organic solution to remove unexposed areas of photoresist and produce a functioning mold.

Figure S2 Analysis of Curve Fitting Routines.

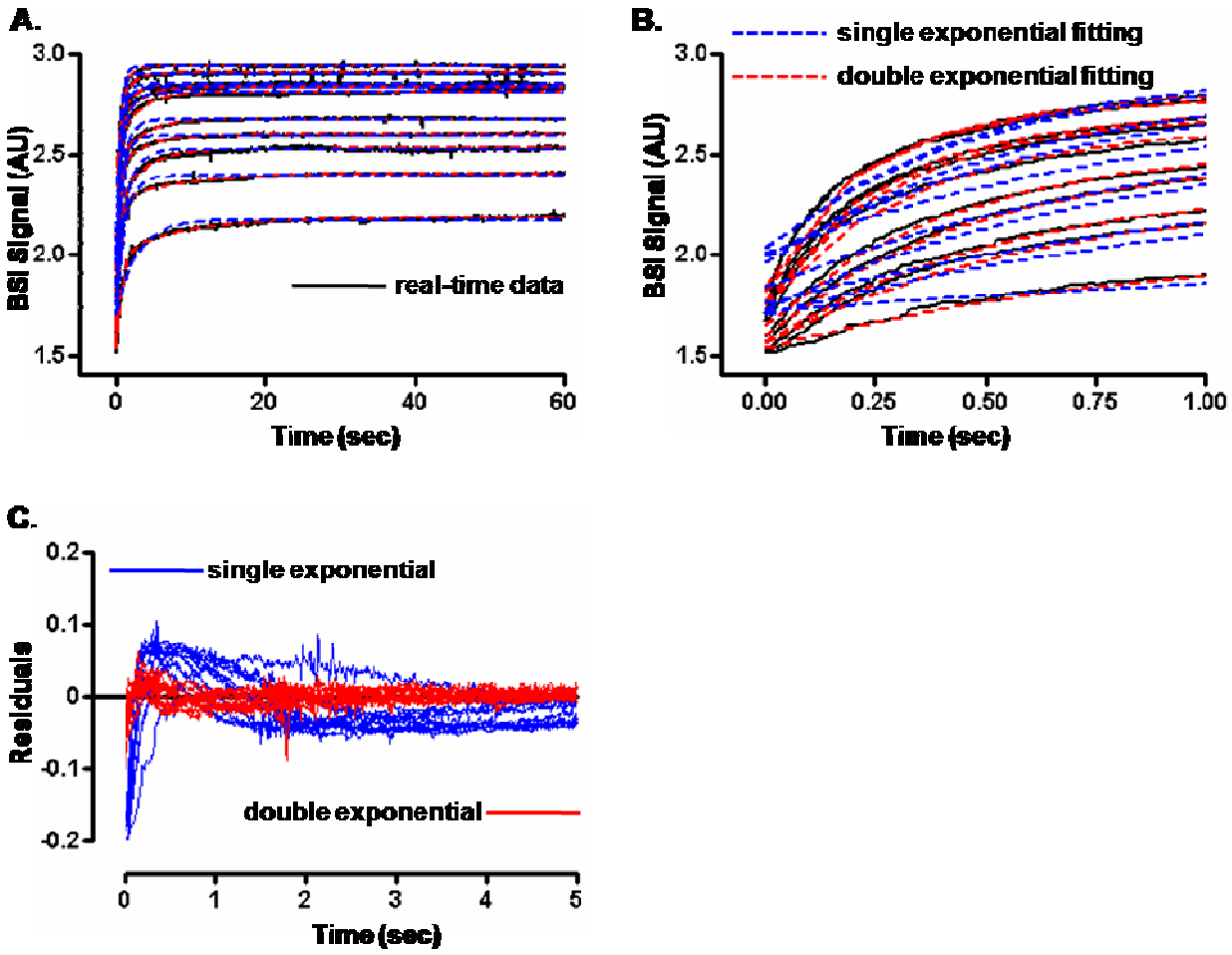

Figure S2 Analysis of Curve Fitting Routines.

(A) Real-time kinetic data (—) from the interaction of αB-D3 and T4L-L99A was recorded by BSI and fit to a single (- - -) and double (- - -) exponential function. (B) The single exponential fitting routine had difficulty not only following the sharp initial rise in signal but also the original starting values. (C) Error analysis of each fitting routine again clearly demonstrates the double exponential is more apt at accurately describing the sHSP●T4L binding event.

Figure S3 BSI Setup.

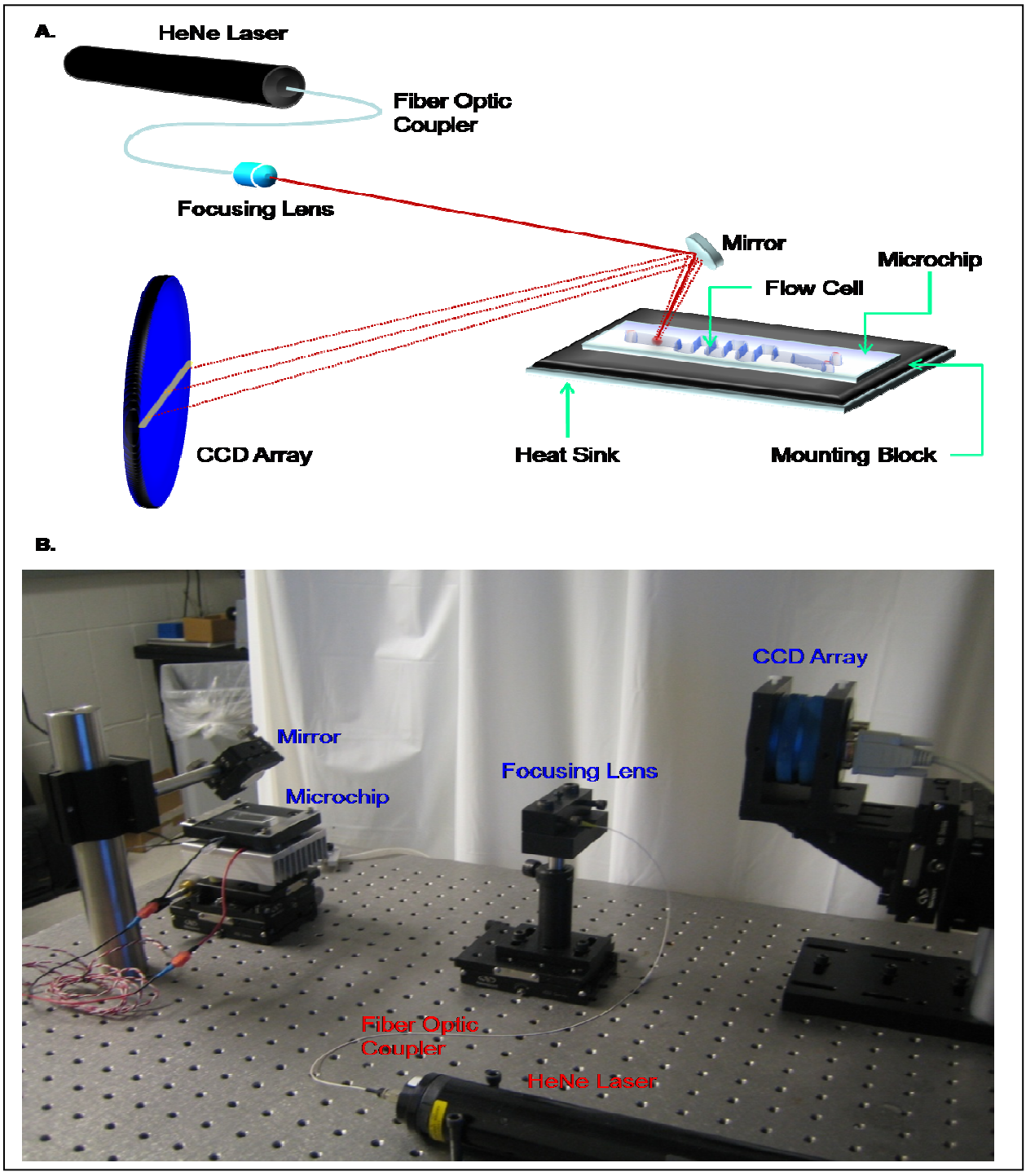

Figure S3 BSI Setup.

(A) A cartoon schematic of the BSI experimental setup is shown. BSI consists of a simple optical train with three main components: a coherent light source, a flow cell, and a phototransducer. (B) A digital image of a working BSI setup is shown.

SECTION 1. MICROCHIP FABRICATION

Optical Lithography. CleWin 2.7 layout editor software was used to design the fluidic network. A soda lime/chrome mask was generated from this design by Delta Mask (The Netherlands) where the chrome layer was ~ 100 nm in thickness. Master molds were created from the lithographic mask by standard optical (Figure S1) and soft lithographic techniques. Three inch silicon wafers (P <100>) were RCA cleaned, dried under N_2 gas and placed on a hot plate at 95°C for 5 minutes just prior to resist deposition. The negative photoresist SU-8 2050 from Microchem (Newton, MA) was evenly deposited on the Si wafer using a Laurell WS-400 Bench-top single wafer spinner. A few milliliters of the resist were poured onto the center of the wafer and spinning commenced for 15 seconds at 500 rpm to spread the photoresist. The speed of the wafer was then increased to 3000 rpm for 30 seconds to form a homogeneous coating. The wafer was then removed from the spin coater and placed on a hot plate for a soft bake (3 min @ 65°C $\Rightarrow$ 9 min @ 95°C). The wafer was then allowed to cool to room temperature. UV exposure through the photolithographic mask for ~15 seconds was accomplished using a NOVACURE 2100 curing system coupled to a liquid wave guide. The liquid wave guide was interfaced with a Karl Suss mask aligner to aid in positioning the lithographic mask. Following irradiation, a post exposure bake (PEB) was performed (1 min @ 65°C $\Rightarrow$ 7 min @ 95°C). The wafer was again cooled to room temperature. Unexposed areas of SU-8 photoresist were removed by immersion in an organic developer from Microchem followed by drying under N_2 gas. Isopropyl alcohol (IPA) was used to ensure the wafer was completely developed. IPA will form a milky white substance on the wafer if any unexposed photoresist remains indicating the developing time should be extended. A hard bake (~5 hours @ 200°C) of the master was performed to further increase mechanical stability resulting in a functional positive relief mold. An Alphastep 200 stylus surface profiler (Tencor Instruments) was used to accurately measure the height of the standing relief structures.

Soft Lithography. All sHSP assays were performed in microchips created by cast molding onto the master mold fabricated above. Cast molding was performed using a silicon elastomer, polydimethylsiloxane (PDMS), purchased as Sylgard 184 (Dow Corning, Midland, MI). Prior to casting, the PDMS was mixed in a 7 : 1 ratio (base : curing agent) and degassed. PDMS was cast over the master that had been placed into a 100 × 15 mm Falcon Petri dish (Becton Dickinson, Franklin Lakes, NJ)

such that the height of the PDMS was ~ 2mm. The Petri dish was placed into a desiccator and a vacuum was applied for further degassing. Once no air bubbles were visibly present, the Petri dish was removed from the desiccators and set in a large convection oven for roughly 8 hours @ 65°C.

After the curing process was complete, the Petri dish was removed from the oven and allowed to cool briefly. The PDMS microchip device was physically removed from the Si master mold by fine precision scalpel and tweezers. Access ports for sample introduction (2 ports) and applied vacuum/waste removal (1 port) were mechanically punched out by stainless steel capillary tubing. PDMS, with the fluidic network facing up, was then plasma oxidized for ~ 10 sec along with a 3″ × 1″ × 1 mm microscope glass slide (Fisher Scientific) cleaned in piranha solution. Following oxidation, the PDMS was irreversibly sealed to the microscope slide so that the fluidic network was in contact with the glass. Water was kept in the channels until experiments were run to help maintain the hydrophilic surface created by plasma oxidation.

SECTION 2. DATA ANALYSIS

Curve Fitting. Kinetic curves from αB-D3 binding T4L-L99A were fit to single and double exponentials (Figure S2A). As demonstrated in Figure S2, the higher ordered function provided a statistically significant improvement in describing the kinetic data of αB-D3 binding T4L-L99A. The single exponential particularly failed to follow the initial ascent and sudden plateau of the binding data as well as greatly miscalculating initial starting values (Figure S2B). Further, examination of the residuals (Figure S2C) clearly indicates the single mode formalism developed earlier[1] is inadequate to accurately represent the complex interaction of sHSP binding assays. A comparison of the error analyses for each fitting routine via F test resulted in the rejection of the single exponential fit at 99% confidence. This outcome indicated BSI is detecting a bi-modal molecular interaction with two separate kinetic events, reinforcing the multifaceted sHSP binding model proposed earlier.[2]

Steady-state Evaluation. Fluorescence and calorimetry were employed to compare and cross-validate data obtained from BSI experiments. To minimize variances between methods, experimental conditions were kept constant across platforms. Binding of αB-D3 to T4L-L99A was monitored by each technique at 37°C and in a buffered solution at pH = 7.2. For fluorescent experiments, monobromobimane was derivatized to our proteins of interest and served as the signaling moiety. While

ITC and BSI do not require the use of a fluorophore for signal detection, the same fluorescently labeled proteins were used in these techniques so as to best mimic the experimental conditions in our fluorescent studies.

The equilibrium dissociation constant (K_D), a measure of binding affinity and thus a description of the molecular interaction can be quickly and simply determined from steady-state values.[3] For consistency, the bi-modal binding formalism used previously[2] to obtain thermodynamic data from steady-state sHSP●T4L fluorescent experiments was applied to our BSI data. However, due to the nature of BSI, certain components of the overall signal must be addressed before quantitative thermodynamic data can be obtained.

Typically in steady-state binding experiments, an initial starting value or baseline can be subtracted from the end-point value to obtain an overall signal with an absolute magnitude. This absolute signal is acquired for multiple receptor●ligand solutions with varying concentration ratios in order to calculate K_D. In our BSI experiments, multiple components can contribute to both the baseline and end-point value. The initial values from our BSI data arise from a combination of buffer, T4L, and sHSP. The concentration of αB-D3 was held constant during these BSI binding assays and the same buffer was used for each component. Yet, as seen in Figure 1c, the starting values for αB-D3 binding T4L-L99A increased linearly. A plot of the initial values versus the concentration of T4L-L99A had the same slope as a calibration curve for T4L-L99A with only a slight increase in the y-intercept of the line (Figure 1c). The increase in the y-intercept value was assigned to the constant signal of αB-D3 and was henceforth subtracted from the overall BSI signal. The linear escalation of starting values is thus attributed to an increase in the free T4L concentration.

In a typical binding curve, where the signal is only due to bound ligand, a binding curve should reach a plateau. The end point values observed in our BSI studies are a resultant of free T4L (both folded and unfolded) and any changes in the system due to the binding of T4L to sHSP. Any differences in the signal between folded and unfolded T4L are assumed to be small relative to the signal due to binding. The presence of a signal proportional to the free ligand concentration however leads to an increasing slope in the end point values we detected. Consequently, our BSI data for αB-D3 binding T4L-L99A failed to reach saturation at high concentrations of T4L (Figure 1b). Nevertheless, just as with the

linear increase in starting values, a T4L calibration curve can be used to perform a 'background subtraction' producing a corrected BSI signal that is shown to reach saturation (Figure 1d). This corrected signal can then be fit to routinely utilized binding equations for the determination of K_D.

Based on the *law of mass action* and assuming our reactions reached equilibrium, the amount bound, L_{Bi}, for species i can be calculated from a simple binding equation:

$$L_{Bi} = \frac{n_{Ti} \times L_F}{K_{Di} + L_F} \qquad \text{Eqn. 1}$$

where n_{T_i} is the total number of binding sites for species i. This reflects the sHSP concentration and the intrinsic number of binding sites per monomer n_i (Figure 1a, eqn. 3). L_F is the free ligand concentration and K_{Di} is the dissociation constant for species i with the number of species used being 1 or 2. The signal is then calculated according to:

$$S_T = S_i L_{Bi} + S_F L_F \qquad \text{Eqn. 2}$$

where S_T is the total signal, S_i is the signal for bound species i, S_F is the signal for free ligand, and L_{Bi} and L_F are described above. Equations 1 and 2 can then be used to fit our corrected steady-state data to determine the values S_F, S_i, and K_{Di}. The binding site variable, n_i, however is not allowed to float. The reason values were chosen for the number of binding sites instead of allowing them to float is due to the interdependence of the parameters. Only the combined value of the two parameters, S_i and n_i, in conjunction with the chaperone concentration, $S_i \times n_i \times R_T$, is uniquely defined in the fits. Therefore, without any other method of determining either of these parameters individually, they are undefined. Values for the number of binding sites were based on previous analyses of T4L binding sHSP.[2] Based on fixing n_i to previously determined values, the equilibrium dissociation constants measured from the steady-state analysis of BSI data were in agreement with those determined by fluorescence and ITC (Table 1). In fact, the presence of two binding components that was apparent in previous fluorescent sHSP binding assays[2] (but unable to be determined) were calculated by BSI, though without the ability to determine n_i values directly from the data.

Global Analysis. The kinetic derivation arrived at in earlier BSI experiments fails to correctly describe the kinetics of our sHSP binding assays as the assumption of $[L] > [R]$ is invalid across the entire data set. Based on previous results, our working hypothesis was sHSP has a high and low affinity for binding partners. Therefore a bi-modal binding mechanism was proposed. This binding formalism can be described with the generic interaction:

$$\begin{aligned} R_1 + L_F &\leftrightarrow L_{B1} \\ R_2 + L_F &\leftrightarrow L_{B2} \end{aligned} \qquad \text{Eqn. 3}$$

where R_i is the amount of free sHSP binding sites per monomer for species i, L_F is the amount of free ligand, and L_{Bi} is the amount of ligand bound for species i. The rate equations describing this bi-modal kinetic interaction are:

$$\frac{dL_f}{dt} = -(k_{f1}R_1 + k_{f2}R_2)L_F + (k_{r1}L_{B1} + k_{r2}L_{B2}) \qquad \text{Eqn. 4}$$

$$\frac{dL_{B1}}{dt} = k_{f1}R_1L_F - k_{r1}L_{B1} \qquad \text{Eqn. 5}$$

$$\frac{dL_{B2}}{dt} = k_{f2}R_2L_F - k_{r2}L_{B2} \quad , \qquad \text{Eqn. 6}$$

$$\frac{dR_1}{dt} = k_{f1}R_1L_F + k_{r1}L_{B1} \qquad \text{Eqn. 7}$$

$$\frac{dR_2}{dt} = k_{f2}R_2L_F + k_{r2}L_{B2} \qquad \text{Eqn. 8}$$

where k_{fi} and k_{ri} are the forward and reverse rates of the binding reactions in Equation 3 respectively. The forward and reverse rates can be determined for each individual trace in the sHSP binding assay. Thus multiple K_D values can be calculated for each trace in the data set. However these calculated K_D values represent a best scenario for one trace only and may not accurately symbolize a comprehensive result. Instead, here all traces were fit simultaneously to one set of parameters in order to minimize a global error function, χ^2. Commonly referred to as global analysis[4], this strategy reduces the effects of instrumental artifacts in a particular kinetic trace on the final parameters and overcomes the uneven sensitivity at either extreme of molar ratios. This method for kinetic analysis was used in distinguishing binding affinities for two destabilized mutants of T4L (Table 2) and to compare the kinetics (Figure 4c) of

a crystallin●crystallin interaction observed by BSI with published results using surface plasmon resonance (SPR). Error analysis for the global fitting routine was carried out by fixing one variable and allowing the remaining variables to minimize the fit to the data.[5] The statistical significance between fits and error determination for individual parameters were done with an F-test.[5]

SECTION 3. ITC EXPERIMENTAL

A MicroCal VP-ITC (Isothermal Titration Calorimetry) was employed to cross validate results obtained by BSI. Solutions of αB-crystallin and T4L-L99A were buffered with 0.15M $Na_2H_2PO_4$, 0.1M KCl, 0.1mM EGTA, and 0.1% sodium azide. Analytes were kept on ice before the experiment and allowed to warm near the experimental temperature prior to sample introduction. All solutions were filtered through a 0.2 micron disc and degassed before calorimetric experiments. αB-crystallin (~ 1.4 mL) was housed in the sample cell for ITC experiments and had an initial concentration of 12 μM. The buffer solution was kept in the reference cell. Approximately 260 μL of T4L-L99A at a concentration equal to 120 μM was drawn into a syringe housed within an automated pipette system. The syringe was placed in the sample cell and spun at 300 RPM. The system was allowed to equilibrate for roughly 2 hours. Once no drift was observed in the baseline and the temperature remained fairly constant, an automated injection sequence was initiated. 10 μL of the T4L mutant was injected into the sample cell containing αB-crystallin twenty-five times with ~ 7 minutes allowed between injections to bring the signal back to baseline. The heat evolved after each injection was recorded and experimental data was analyzed by Origin software to calculate thermodynamic parameters for comparison to BSI and fluorescence experiments.

SECTION 4. BSI EXPERIMENTAL

The experimental setup for multiple embodiments of BSI has been described exhaustively elsewhere.[1, 6, 7] As shown in Figure S3, a focusing lens (Oz Optics, Ontario, Canada) with a 283 mm working distance was fiber optically coupled to a 5mW, 632.8 nm HeNe laser (Melles Griot, Carlsbad, CA). The output beam was directed onto a microchip molded in PDMS using a highly reflective (> 99%) aluminum mirror. The mirror above the PDMS chip was positioned so that the incident beam was directed onto the flow channel orthogonal to fluid flow. The angle of the mirror and the correct working distance ensure parallel rays impinge the channel. The proper working distance was measured both physically and by adjusting the reflected laser spot size in the far field. When properly aligned, the spot

size of the laser beam at the channel was calculated to have a diameter of 100 μm. The PDMS microchip was securely mounted on top of an aluminum block. Solutions were kept on ice during the experiment and briefly allowed to warm to room temperature prior to their introduction into the microchannel. Experimental temperatures were maintained by a thermoelectric cooler (Peltier device) connected to a Melcor temperature controller (MELCOR, Trenton, NJ). The microchip assembly was connected to two translation stages which allow movement of the chip in both x and y directions. A portion of the high resolution backscattered interference pattern produced upon the interaction of light with the microchip was directed by the same mirror onto a GARRY 3000 CCD array (Ames Photonics, Hurst, Texas) functioning as a position sensing transducer. The CCD array contains 3000 pixels with each pixel 7 μm wide, 200 μm tall, and having 7 μm center-to-center spacing. The array has a total length of 21 mm and has a pseudo-Gaussian spectral response from 350 – 1100 nm with its quantum efficiency centered near 500 nm. Binding experiments were monitored in real-time at frequencies ca. 50-100 Hz.

The laser and temperature controller were powered on and allowed to equilibrate over a one hour period prior to starting any experiments. The centroid of the backscattered interference pattern was located just above the focusing lens insuring that the alignment of the system was along a central plane. The CCD array was positioned near direct backscatter in order to capture the most spatially sensitive section of the interference pattern.[1] Typically, the edge of the CCD array was positioned to capture the 5^{th} or 6^{th} constructive interference fringe from the centroid and outward. Although simulated fringes nearest direct backscatter produced larger spatial shifts with changes to the optical pathlength, a balance between sensitivity and the working conditions of the system must be met when aligning the CCD near the centroid. Light intensity near direct backscatter is extremely high and must be attenuated so as to not saturate the detector. However, in doing so, the only fringe that remains detectable in the current setup is the centroid, negating the need and advantages of the large area CCD array and FFT algorithm. Also, the interference fringes near direct backscatter are less sinusoidal and resemble more of a damped oscillator or Bessel function degrading the FFT output and making the determination of a dominant spatial frequency troublesome. Furthermore, the frequencies that are easily quantified in the magnitude spectrum of the FFT at positions very close to the centroid are often times masked by DC noise.

REFERENCES

(1) Bornhop, D. J.; Latham, J. C.; Kussrow, A.; Markov, D. A.; Jones, R. D.; Sorensen, H. S. *Science* **2007**, *317*, 1732-1736.
(2) Sathish, H. A.; Stein, R. A.; Yang, G.; McHaourab, H. S. *J Biol Chem* **2003**, *278*, 44214-44221.
(3) Motulsky, H.; Christopoulos, A. *Fitting Models to Biological Data Using Linear and Nonlinear Regression*; Oxford Univeristy Press: New York, 2004.
(4) Beechem, J. M. *Biophys J* **1998**, *74*, 2141.
(5) Rousseau, D. L., Jr.; Staros, J. V.; Beechem, J. M. *Biochemistry* **1995**, *34*, 14508-14518.
(6) Swinney, K.; Markov, D.; Bornhop, D. J. *Analytical Chemistry* **2000**, *72*, 2690-2695.
(7) Wang, Z. X.; Jiang, R. F. *Febs Letters* **1996**, *392*, 245-249.

* Supporting Information Available: This material is available free of charge via the Internet at http://pubs.acs.org